Extreme Mechanics Letters 18 (2018) 36–44

Contents lists available at ScienceDirect

Extreme Mechanics Letters

journal homepage: www.elsevier.com/locate/eml

Metadamping and energy dissipation enhancement via hybrid phononic resonators

D. DePauw, H. Al Ba'ba'a, M. Nouh *

Department of Mechanical & Aerospace Engineering, University at Buffalo (SUNY), Buffalo, NY, United States

ARTICLE INFO

Article history:
Received 31 August 2017
Received in revised form 21 October 2017
Accepted 4 November 2017
Available online 10 November 2017

ABSTRACT

A novel metamaterial configuration is presented that combines hybrid attributes from acoustic metamaterials and phononic crystals. The dispersion characteristics of the system, referred to as the phononic resonator (PR), is shown to vary across a wide spectrum of behaviors that can, via optimal selection of inertial and stiffness parameters, be tuned to resemble a locally resonant mechanism, a phononic system, as well as a uniform homogeneous lattice. When coupled with damping elements, the emergent dissipative effect, known as the metadamping phenomenon, of the PR is shown to exceed that of a statically equivalent acoustic metamaterial under certain conditions which are highlighted here. The metadamping amplification is verified in finite PR systems via a power flow approach that depicts the spatial rate of energy dissipation along the length of a 100 cells phononic resonator.

1. Introduction

The physics of periodic structures have received considerable attention lately owing to their unique abilities to manipulate elastic wave propagation within their media [1]. Such abilities culminate in intriguing features including band gaps (frequency ranges of blocked wave propagation) [2,3], directional patterns [4,5], and amplified energy dissipation [6,7]. As such, periodic structures with unconventional dispersive characteristics have been mostly classified into two main categories: Phononic Crystals (PCs) and Acoustic Metamaterials (AMs). Both categories have been heavily investigated in the context of discrete (spring–mass) systems [8–11], bars [12–15], flexural beams [16–18] and plates [19–22].

The interplay between wave dispersion in periodic systems and material and/or viscous damping have been shown to onset interesting traits [23–28]. One of these is the generation of enhanced damping properties, or *metadamping*, that goes beyond the conventional dissipation provided by the damping elements. The emergence of metadamping in an AM in particular has been shown to quantitatively yield higher damping ratios across the entire wavenumber spectrum when compared to a statically equivalent PC with an identical damping amount [6]. Wave propagation in periodic systems is modeled using their derived dispersion equations which relate the spatial and temporal properties of the propagating waves. Such relations are typically obtained from the dynamics of an individual unit cell using the Bloch solution which assumes an infinite chain of cells [29,30]. The output is a band structure that graphically relates the incident frequency ω to the wavenumber β. A PC unit cell comprises a discrete change in inertial and elastic properties which results in Bragg-type band gaps (Fig. 1a) [31]. An AM's unit cell consists of a base structure that houses a local resonator that contributes to the rise of lower frequency, yet narrower, band gaps [8,32] (Fig. 1b).

Periodic systems that combine elements of phononics and locally resonant mechanisms have been, at times, shown to acquire novel dispersion features or drastically improve current ones [33–35]. In this letter, we report the dispersion as well as dissipative characteristics of a hybrid phononic system that comprises a base cell that houses a resonant substructure that is locally connected to the adjacent cell, rather than being isolated. As depicted in Fig. 1c, the hybrid system (referred to here as a Phononic Resonator (PR) for brevity) represents a wide spectrum of physical design choices. The traditional PC and AM represent two distinct data points on the opposing spectrum ends and can be realized by setting k_a and one of the k_b springs to zero, respectively. The dampers $c_{a,b}$ are added to characterize the energy dissipation in the PR which is shown to exercise significantly greater metadamping effects than both the PC and the AM with the suitable choice of parameters. The effectiveness of the PR's enhanced damping ratio is mathematically quantified and correlated to the mass and stiffness ratios of the structure.

* Corresponding author.
E-mail address: mnouh@buffalo.edu (M. Nouh).

https://doi.org/10.1016/j.eml.2017.11.002
2352-4316/

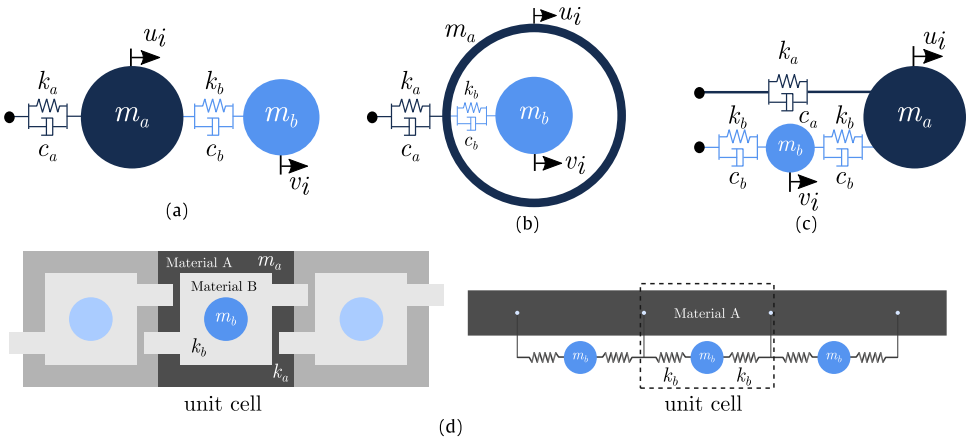

Fig. 1. Discrete realizations of (a) a Phononic Crystal (PC), (b) an Acoustic Metamaterial (AM) , and (c) a Phononic Resonator (PR). (d) Different possible continuous realizations of the PR system.

2. Dispersion relations

2.1. Mathematical formulation

The displacements u_i and v_i of the ith cell of a phononic resonator (PR), as highlighted in Fig. 1c are governed by the equations of motion given by

$$m_a\ddot{u}_i + c_a(2\dot{u}_i - \dot{u}_{i+1} - \dot{u}_{i-1}) + k_a(2u_i - u_{i+1} - u_{i-1}) - c_b(\dot{v}_{i+1} + \dot{v}_i - 2\dot{u}_i) - k_b(v_{i+1} + v_i - 2u_i) = 0 \quad (1a)$$

$$m_b\ddot{v}_i + 2c_b\dot{v}_i + 2k_bv_i - c_b(\dot{u}_{i-1} + \dot{u}_i) - k_b(u_{i-1} + u_i) = 0 \quad (1b)$$

and its dispersion relations can be obtained by assuming a generalized Bloch solution of the form

$$u_{i+r} = \tilde{u}e^{\mathbb{i}r\bar{\beta}+\lambda t} \quad (2)$$

and similarly for v_{i+r}. In Eq. (2), $\tilde{u}$ is the complex wave amplitude, and λ is a frequency function, which is a complex quantity for damped systems and equivalent to $\mathbb{i}\omega$ for undamped ones, $\bar{\beta} = \beta\ell$ is the dimensionless wavenumber, ℓ is the cell spacing, $r = -1, 0, 1$, and $\mathbb{i} = \sqrt{-1}$. By substituting Eq. (2) in (1), and with some additional manipulations [6], the dispersion relation can be obtained as

$$\bar{\lambda}^4 + \bar{a}\bar{\lambda}^3 + \bar{b}\bar{\lambda}^2 + \bar{c}\bar{\lambda} + \bar{d} = 0 \quad (3)$$

where $\bar{\lambda} = \frac{\lambda}{\omega_0}$. Eq. (3) is normalized using $\omega_0 = \sqrt{\frac{k_b}{m_b}}$ and the following non-dimensional quantities: the mass ratio $\mu = \frac{m_b}{m_a}$, the stiffness ratio $\kappa = \frac{k_b}{k_a}$, $\gamma = \frac{\mu}{\kappa}$, the local damping ratios $\zeta_a = \frac{c_a}{2\sqrt{m_ak_a}}$ and $\zeta_b = \frac{c_b}{2\sqrt{m_bk_b}}$. It is worth noting that this dispersion relation is the same for an AM and a PC with different expressions of $\bar{a}$, $\bar{b}$, $\bar{c}$ and $\bar{d}$. The summary of these parameters for the three systems (PC, AM, and PR) are listed in Table 1.

2.2. Behavior of an undamped PR

For an undamped PR, $\zeta_a = \zeta_b = 0$ and consequently Eq. (3) reduces to

$$\Omega^4 - \hat{b}\Omega^2 + \hat{d} = 0 \quad (4)$$

where $\Omega = \frac{\omega}{\omega_0}$, $\hat{b} = 2(1+\mu)+2\gamma\alpha$ and $\hat{d} = (4\gamma+2\mu)\alpha$. The upper (optic) dispersion branch given by Eq. (4) can be manipulated by changing the PR's system parameters such that it resembles either a PC or an AM with a turning point in between. The difference between the optic branch of PC and AM is the group velocity (i.e. the branch's slope) where the AM and the PC possess positive and negative group velocities, respectively. The turning point can be analytically obtained by equating the roots of the optic branch in Eq. (4) at $\bar{\beta} = 0$ and $\bar{\beta} = \pi$ which are given by $\Omega = \sqrt{2(\mu+1)}$ and $\Omega = \sqrt{2\mu(\frac{2}{\kappa}+1)}$. By equating these roots, it can be shown that $2\mu = \kappa$ is the relation that governs this AM-to-PC performance switch. If $2\mu > \kappa$, the branch behaves in a manner consistent with AMs while for $2\mu < \kappa$, it resembles the optic branch of a PC. One of the band gap limits is always at $\Omega = \sqrt{2}$ while the other occurs at $\Omega = \sqrt{2\mu(\frac{2}{\kappa}+1)}$ or $\Omega = \sqrt{2(\mu+1)}$ depending on whether the system is behaving similar to a PC or an AM, respectively. It is worth noting that while the PR behaves like a PC, it is possible for $\Omega = \sqrt{2\mu(\frac{2}{\kappa}+1)}$ to be either greater than or less than $\sqrt{2}$, which indicates that the root may appear in either the optic or acoustic branches. Investigating the special case $2\mu = \kappa$ reveals some interesting characteristics of the PR's dispersive behavior. In such a case, the optic branch reduces to a flat line indicating a natural frequency of the system located at $\Omega = \sqrt{2+\kappa}$. Moreover, the band gap in this case ceases to exist and an unbounded stop band starts immediately after $\Omega = \sqrt{2}$. Furthermore, the PR can be tuned to behave similar to a band gap free homogeneous lattice given the right choice of parameters. Such a condition is satisfied when the optic and the acoustic branches at $\bar{\beta} = \pi$ coincide, i.e. when the discriminant of Eq. (4) is equal to zero. This condition can be shown to happen when $\mu = \frac{\kappa}{\kappa+2}$ or $\kappa = \frac{2\mu}{1-\mu}$. Fig. 2 graphically summarizes all of the aforementioned scenarios.

To further understand the behavior of a PR's band structure, we consider the driven wave problem where Eq. (4) is reformulated in terms of $\bar{\beta} = \cos^{-1}\Phi$ with

$$\Phi(\Omega) = 1 - \frac{\kappa}{2\mu}\frac{\Omega^4 - 2(1+\mu)\Omega^2}{\Omega^2 - (2+\kappa)} \quad (5)$$

It can be inferred from Eq. (5) that the resultant wavenumber is complex (indicating a band gap) for $|\Phi| > 1$. By setting $\frac{\partial\Phi}{\partial\Omega} = 0$, the roots $\hat{\Omega}$ can be obtained which are indicative of maximum attenuation frequencies or inflection points, given by

$$\hat{\Omega}_{\pm}^2 = (2+\kappa) \pm \sqrt{(2+\kappa)(\kappa-2\mu)} \quad (6)$$

As evident in Eq. (5), and confirmed by Fig. 2, it can be observed that $\Omega = \sqrt{2+\kappa}$ is a point of discontinuity which also happens to be a point of maximum attenuation when the discriminant of Eq. (6) is zero. This point is found to be equivalent to the resonance frequency denoted $\hat{\Omega}_R$ in Fig. 2. With $\hat{\Omega} = \sqrt{2+\kappa}$ and revisiting

Table 1
$\bar{a}$, $\bar{b}$, $\bar{c}$ and $\bar{d}$ in Eq.(3) for all systems, where $\alpha = (1 - \cos\bar{\beta})$.

	PR	PC	AM
$\bar{a}$	$4\zeta_b(1+\mu)+4\zeta_a\sqrt{\gamma}\alpha$	$2(1+\mu)(\zeta_a\frac{\sqrt{\gamma}}{\mu}+\zeta_b)$	$2\zeta_b(1+\mu)+4\zeta_a\sqrt{\gamma}\alpha$
$\bar{b}$	$2(1+\mu)+2(\gamma+8\zeta_a\zeta_b\sqrt{\gamma}+4\mu\zeta_b^2)\alpha$	$(1+\frac{1}{\kappa})(1+\mu)+8\zeta_a\zeta_b\sqrt{\gamma}\alpha$	$(1+\mu)+2(\gamma+4\zeta_b\zeta_a\sqrt{\gamma})\alpha$
$\bar{c}$	$8(\zeta_b\gamma+\zeta_a\sqrt{\gamma}+\zeta_b\mu)\alpha$	$4\sqrt{\gamma}(\zeta_a+\zeta_b\sqrt{\gamma})\alpha$	$4\sqrt{\gamma}(\zeta_a+\zeta_b\sqrt{\gamma})\alpha$
$\bar{d}$	$(4\gamma+2\mu)\alpha$	$2\gamma\alpha$	$2\gamma\alpha$

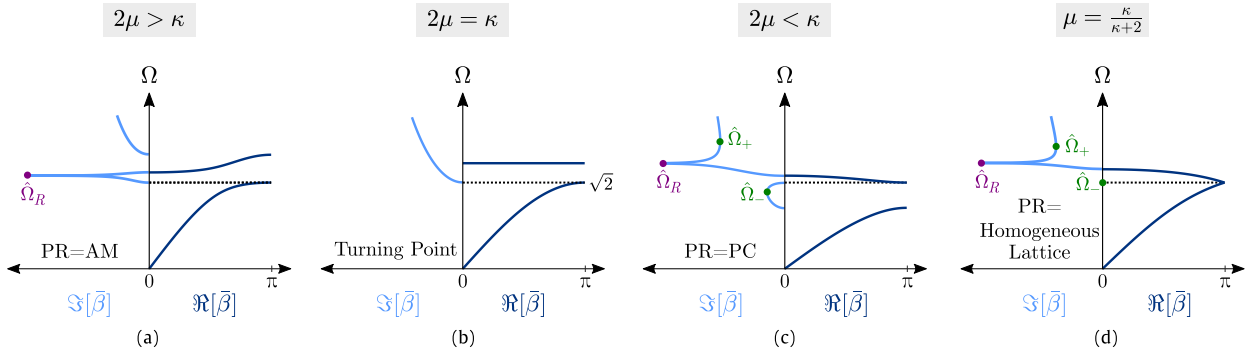

Fig. 2. Dispersion relations of the PR at the different mass and stiffness ratios, μ and κ, combinations: (a) $2\mu > \kappa$, (b) $2\mu = \kappa$, (c) $2\mu < \kappa$, and (d) $\mu = \kappa/(\kappa+2)$.

the case where $2\mu = \kappa$, Eq. (5) reduces to $(1 - \Omega^2)$ which explains the lack of an $\hat{\Omega}_R$ in Fig. 2b. For $2\mu > \kappa$, Eq. (6) yields complex roots which explains the lack of maximum attenuation or inflection points besides $\hat{\Omega}_R$ in Fig. 2a. In Fig. 2c where $2\mu < \kappa$, $\hat{\Omega}_+$ is an inflection point in the stop band region while $\hat{\Omega}_-$ dictates the location of the maximum attenuation of the Bragg band gap. The latter vanishes when the PR behaves similar to a homogeneous lattice at $\mu = \frac{\kappa}{\kappa+2}$, at which case the inflection point is located at $\hat{\Omega}_+ = \sqrt{2(1+\kappa)}$ as demonstrated in Fig. 2d.

2.3. Negative effective mass

Since the PR exhibit a dispersion behavior similar to the AM, it is naturally of interest to examine the effective mass of the unit cell as a function of the frequency and how it compares to the band gap location. If the mass m_b and its stiffness k_b are assumed to be embedded within the mass m_a, the unit cell can be seen as a single effective mass m_e with a spring of stiffness k_a. Knowing that the dispersion relation of a single spring–mass with spring k_a and mass m_e is $\omega = \sqrt{2k_a\alpha/m_e}$ [25], it immediately follows that $\alpha = \frac{\omega^2 m_e}{2k_a} = \frac{\Omega^2\kappa\bar{m}_e}{2}$, where $\bar{m}_e = \frac{m_e}{m_a}$ is the nondimensional effective mass. Substituting α back into Eq. (4) and rearranging the equation in terms of $\bar{m}_e$, we obtain:

$$\bar{m}_e = \frac{2(1+\mu) - \Omega^2}{(2+\kappa) - \Omega^2} \tag{7}$$

Eq. (7) results in a negative effective mass if the numerator and denominator have different signs. Interestingly, the PR will always exhibit a negative effective mass at a certain range of frequencies whether it behaves as a PC or AM, but the negative mass coincides with the band gap region only when it behaviors as an AM and lies in the unbounded stop band region when it behaves as a PC. A spacial case is the turning point of $2\mu = \kappa$, where the effective mass is neutralized and its value becomes $m_e = 1$ as a result of the numerator and denominator cancellation. Fig. 3 shows the dispersion curves (1st column) and the corresponding effective mass (2nd column) as a function of frequency for (a) $\mu = 0.5$ and $\kappa = 0.05$ where PR behaves as an AM and (b) $\mu = 0.2$ and $\kappa = 1$ where in it acts as PC.

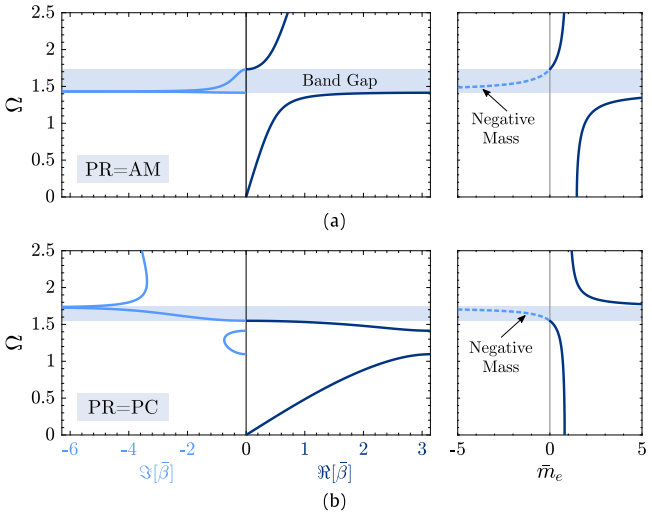

Fig. 3. The dispersion curves (1st column) and effective mass (2nd column) plots for (a) $\mu = 0.5$ and $\kappa = 0.05$ and (b) $\mu = 0.2$ and $\kappa = 1$. PR behaves as an AM in (a) while in (b) it behaves as PC.

2.4. Long wave speed

In order to accurately evaluate the performance of a PR as it compares to a PC and an AM, the three systems under consideration should be statically equivalent, i.e. exhibit an identical long wave speed c_{stat}. As such, analytical expressions of c_{stat} for the three systems are derived from their respective dispersion relations using Taylor series expansions and binomial approximations around $\bar{\beta} = 0$. The detailed derivations are provided in the Appendices. For brevity, the final expressions are given by

$$c_{stat}^{PC} = \omega_0^{PC}\ell\sqrt{\frac{\mu}{(\kappa+1)(1+\mu)}} \tag{8}$$

$$c_{stat}^{AM} = \omega_0^{AM}\ell\sqrt{\frac{\mu}{\kappa(1+\mu)}} \tag{9}$$

$$c_{stat}^{PR} = \omega_0^{PR}\ell\sqrt{\frac{\mu(\kappa+2)}{2\kappa(1+\mu)}} \tag{10}$$

Consequently, the three systems will be kept statically equivalent by equating Eqs. (8) through (10). If the mass and stiffness ratios are kept fixed, the values of the different ω_0 have to be appropriately adjusted to maintain the required static equivalence. As a result, the ratio between the different ω_0's can be easily found. Further, the dispersion relations have to be modified to maintain this equivalence throughout the analysis. Following Ref. [6] and choosing a PC system as a starting point, it can be shown that the dispersion relations for the AM and the PR become

$$\bar{\lambda}^4 + \bar{\omega}_0\bar{a}\bar{\lambda}^3 + \bar{\omega}_0^2\bar{b}\bar{\lambda}^2 + \bar{\omega}_0^3\bar{c}\bar{\lambda} + \bar{\omega}_0^4\bar{d} = 0 \tag{11}$$

where $\bar{\lambda} = \frac{\lambda}{\omega_0^{\mathrm{PC}}}$ and $\bar{\omega}_0 = \sqrt{\frac{\kappa}{\kappa+1}}$ and $\sqrt{\frac{2\kappa}{(\kappa+1)(\kappa+2)}}$ for an AM and a PR, respectively. The dispersion relation in Eq. (3) remains the same for the PC. Another means of maintaining static equivalence is by keeping ω_0 fixed for the three systems and adjusting the stiffness and/or mass ratios, κ and μ, accordingly. In this scenario, Eq. (3) can be used as is for all systems. By choosing to fix κ, and again using μ^{PC} as a reference point, it can be shown that $\mu^{\mathrm{AM}} = \frac{\mu^{\mathrm{PC}}\kappa}{1+\kappa+\mu^{\mathrm{PC}}}$ and $\mu^{\mathrm{PR}} = \frac{2\kappa\mu^{\mathrm{PC}}}{(2+\kappa+\kappa^2)\mu^{\mathrm{PC}}+(1+\kappa)(2+\kappa)}$ will guarantee static equivalence. To provide a consistent comparative analysis with the results provided in [6], the first approach will be adopted here.

3. Metadamping enhancement in PRs

3.1. Damping ratio

In this section, we evaluate metadamping in PR systems by comparing the effective damping ratio of the phononic resonator to that of an AM and a PC reported in a benchmark example from literature [6]. The following parameters (arbitrary units) are adopted in the analysis for all three systems: $m_a = 1$, $m_b = 5$ (i.e. $\mu = 5$), $\kappa = 1/5$, $\omega_0^{\mathrm{PC}} = 100$, and $\omega_0^{\mathrm{AM}} = 40.9$. The adjusted ω_0^{PC} is equal to 38.9 resulting in a long wave speed of $c_{stat} = 83.3$. The damping coefficients $c_a = c_b = 40$ are used for all three systems. The local damping ratios ζ_a and ζ_b of the PC as defined earlier are equal to 0.04. To calculate ζ_a and ζ_b corresponding to the AM and PR systems, the following conditions have to be satisfied

$$\zeta^{\mathrm{AM}} = \bar{\mu}^{\mathrm{PC}}_{\mathrm{AM}}\sqrt{\frac{\kappa}{\kappa+1}}\,\zeta^{\mathrm{PC}} \tag{12a}$$

$$\zeta^{\mathrm{PR}} = \bar{\mu}^{\mathrm{PC}}_{\mathrm{PR}}\sqrt{\frac{2\kappa}{(\kappa+1)(\kappa+2)}}\,\zeta^{\mathrm{PC}} \tag{12b}$$

where $\bar{\mu}^{\mathrm{PC}}_{\mathrm{AM}} = \frac{m_b^{\mathrm{PC}}}{m_b^{\mathrm{AM}}}$ and $\bar{\mu}^{\mathrm{PC}}_{\mathrm{PR}} = \frac{m_b^{\mathrm{PC}}}{m_b^{\mathrm{PR}}}$ for the two systems; both equal to 1 in this case. To further ensure a fair comparison, and since a PR comprises one more damper per unit cell, the value of ζ_b^{PR} outputted from Eq. (12b) is multiplied by a factor of 0.5. The dispersion relations of the three systems are computed by implementing Eq. (11) and sweeping the values of the wavenumber $\bar{\beta}$ across one wave cycle, i.e. $\bar{\beta} = 0 \rightarrow \pi$. The solution $\bar{\lambda}$ can then be expressed in the form [6]

$$\bar{\lambda}_s(\bar{\beta}) = -\xi_s(\bar{\beta})\bar{\omega}_s(\bar{\beta}) \pm \mathbb{i}\bar{\omega}_{d_s}(\bar{\beta}) \tag{13}$$

where $\bar{\omega}_s$ and $\bar{\omega}_{d_s}$ are the normalized resonant and the damped wave frequencies, respectively [25] and $s = 1, 2$ refers to the acoustic and optic dispersion branches. $\xi_s(\beta) = -\Re[\bar{\lambda}_s(\bar{\beta})]/|\bar{\lambda}_s(\bar{\beta})|$ is the damping ratio corresponding to each dispersion branch and the combined term $\xi_s(\bar{\beta})\bar{\omega}_s(\bar{\beta})$ is the decay in the wave amplitude with time [25]. The system's total damping ratio ξ_{sum} is given by $\xi^z_{sum}(\beta) = \xi^z_1(\beta) + \xi^z_2(\beta)$, where the index z denotes the system under consideration: PC, AM, or PR. Henceforth, following the constraints enforced earlier related to static equivalency and unifying the damping amount per unit cell, any remaining discrepancies in the damping ratios across the wave number spectrum is a direct indication of the metadamping phenomenon in each system. In other words, systems with higher damping ratios are able to better attenuate incident waves with the same amount of damping as that of a system with a lower one.

Fig. 4 shows the dispersion diagrams as well as the damping ratio variation in all the three systems for (a) the parameters used in the benchmark example: $\mu = 5$ and $\kappa = \frac{1}{5}$ [6] and (b) $\mu = 5$ and $\kappa = 5$. The results of the damped natural frequency ω_d are presented in the dimensional form for comparison purposes, where $\omega_d = \bar{\omega}_d\omega_0^{\mathrm{PC}}$. It is important to note here that the dispersion shape of the damped PR will not necessarily follow the equations developed for the undamped case in Section 2.2. Thus, the results presented here for $\kappa = \mu$ should not be confused with the undamped behavior of the PR when its behavior resembles an AM (Fig. 2a).

From the results, it can be seen that the damping ratio of the AM when $\kappa = 1/5$ is slightly higher than that of the PR and that the damping ratios of both the AM and the PR are higher than that of the PC. The dispersion curves show that the PR, in this case, behaves like an AM. On the other hand, when $\kappa = 5$, the PR's dispersion resembles a PC with an improved damping ratio that exceeds both the AM and the PC. Given that the emergence of metadamping was first reported as a unique qualitative advantage of locally resonant AM systems, this is an interesting result since the enhanced damping performance of the PR demonstrated in this example occurs when the system starts behaving like a PC.

As has been reported in [6], the accumulative effect of the metadamping phenomenon over the entire wavenumber spectrum can be mathematically quantified by the damping emergence metric $\mathbf{Z}^z$ given by the integration

$$\mathbf{Z}^z = \int_0^{\pi} \xi^z_{sum}\, d\bar{\beta} \tag{14}$$

which is most insightful when comparing the differences in the accumulative damping capability of the different designs. These differences can be calculated by subtracting the respective $\mathbf{Z}$'s. For example, the enhancement of a PR's metadamping over a PC is given by

$$\mathbf{Z}^{\mathrm{PR}}_{\mathrm{PC}} = \mathbf{Z}^{\mathrm{PR}} - \mathbf{Z}^{\mathrm{PC}} \tag{15}$$

Therefore, it follows that a negative $\mathbf{Z}^{\mathrm{PR}}_{\mathrm{PC}}$ indicates a metadamping deterioration. Fig. 5 displays provides a comparison of the metadamping metric across the three systems for a wide range of μ and κ combinations, while maintaining the same ζ_a and ζ_b used in Fig. 4. As can be seen from the figure, the metadamping advantage of one design over the other is contingent on the unit cell parameters. Each of the three systems have regions where their damping effectiveness outperforms the other two, except for the PC which can only match the damping emergence in the PR but not exceed it. When comparing AMs to PCs, it can also be seen that the PC will rarely outperform the AM which is consistent with the findings of [6]. On the other hand, when comparing the new PR design to the AM, there are large regions where one design becomes notably more effective in terms of damping capacity.

The results presented in Fig. 5 are all computed with for $\zeta_a = \zeta_b$. Therefore, it is naturally of interest to examine the effects of both ζ_a and ζ_b on the same phenomenon. Fig. 6 displays the effects of varying ζ_a and ζ_b on the metadamping of the different systems for both sets of μ and κ used to generate Fig. 4. The results show that different damping amounts in the system, whichever one it is, may induce larger metadamping emergence but the trends change depending on the mass and stiffness ratios chosen. For all three cases of $\mathbf{Z}$ at $\kappa = 1/5$, a global maximum of the metadamping

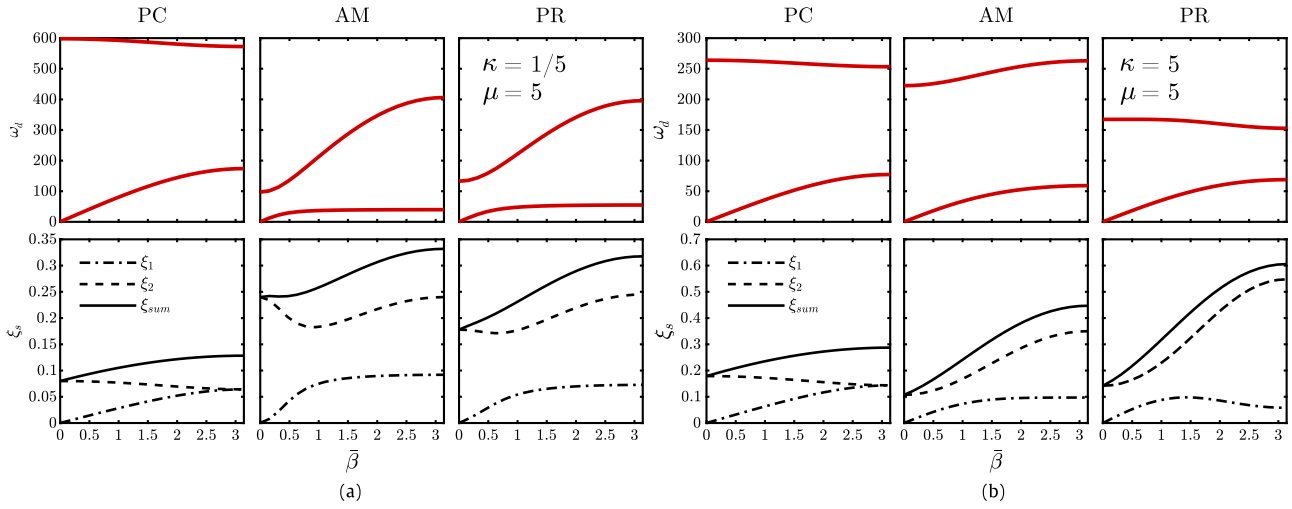

Fig. 4. Dispersion curves for ω_d and ξ_s for a PC, AM, and a PR for $\mu = 5$ and (a) $\kappa = 1/5$ and (b) $\kappa = 5$.

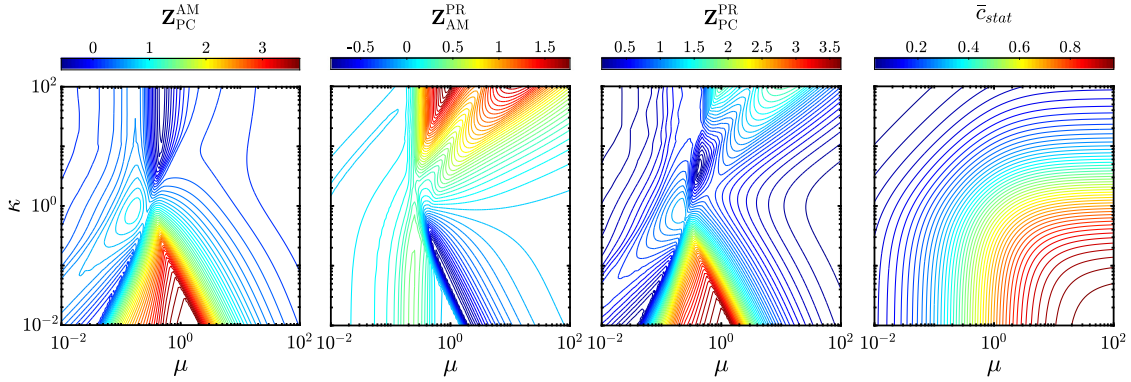

Fig. 5. Comparative evaluation of the metadamping emergence in the three designs. ζ_a and ζ_b equal to 0.04 for all cases. For reference, the normalized long wave speed $\bar{c}_{stat} = \frac{c_{stat}}{\omega_0^{\mathrm{PC}} \ell}$ is displayed in the last column.

phenomenon is found corresponding to a certain optimal ζ_a and ζ_b combination. However, for $\kappa = 5$, $\mathbf{Z}_{\mathrm{AM}}^{\mathrm{PR}}$ and $\mathbf{Z}_{\mathrm{PC}}^{\mathrm{PR}}$ have multiple optimal points. This comparison between the metadamping at $\kappa = 1/5$ and $\kappa = 5$ proves that a deliberate change in the amount of damping injected in the system can have a drastic influence on the resultant metadamping emergence and should, therefore, be considered in the design process.

Finally, we conclude this discussion with an optimization study designed to seek the maximum possible enhancement of the metadamping phenomenon for a given set of μ, κ, ζ_a and ζ_b values. The optimization is performed as follows: for each combination of μ and κ, ζ_a and ζ_b are swept in search for the maximum emergence value similar to Fig. 6. The maximum value of $\mathbf{Z}$ is recorded along with the values of ζ_a and ζ_b that result in this maximum. Fig. 7 shows the results of the optimization process. An interesting observation is that the regions containing the largest metadamping improvement of one design over the other mostly require small values of ζ_a and ζ_b. This implies that the emergence of metadamping in dissipative PCs, AMs, or PRs, is primarily a product of the unit cell dynamics rather than the existing damping elements. It also indicates that the total metadamping amount depends more on the stiffness and mass ratios, κ and μ, as opposed to ζ_a and ζ_b. The optimization results also suggest trends that enable certain designs to be more effective in vibration mitigation applications without necessarily needing heavy material damping which can often be detrimental to the structure's load-bearing capacity. Specifically, in the cases of $\mathbf{Z}_{\mathrm{PC}}^{\mathrm{AM}}$ and $\mathbf{Z}_{\mathrm{PC}}^{\mathrm{PR}}$, larger metadamping can be achieved

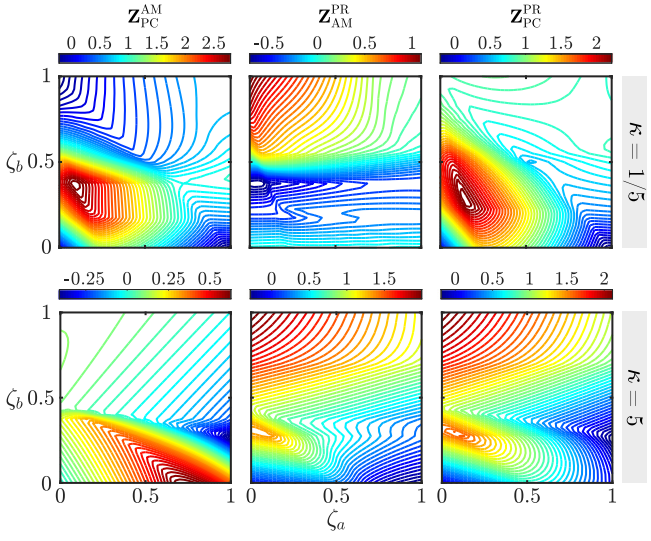

Fig. 6. Evaluation of the metadamping emergence metrics $\mathbf{Z}_{\mathrm{PC}}^{\mathrm{AM}}$, $\mathbf{Z}_{\mathrm{AM}}^{\mathrm{PR}}$ and $\mathbf{Z}_{\mathrm{PC}}^{\mathrm{PR}}$ as a function of ζ_a and ζ_b values for a mass ratio of $\mu = 5$ and two different stiffness ratios: $\kappa = 1/5$ and $\kappa = 5$.

for small values of κ and large values of μ. While in the case of $\mathbf{Z}_{\mathrm{AM}}^{\mathrm{PR}}$, larger metadamping tends to accompany larger values of κ at a given value of μ.

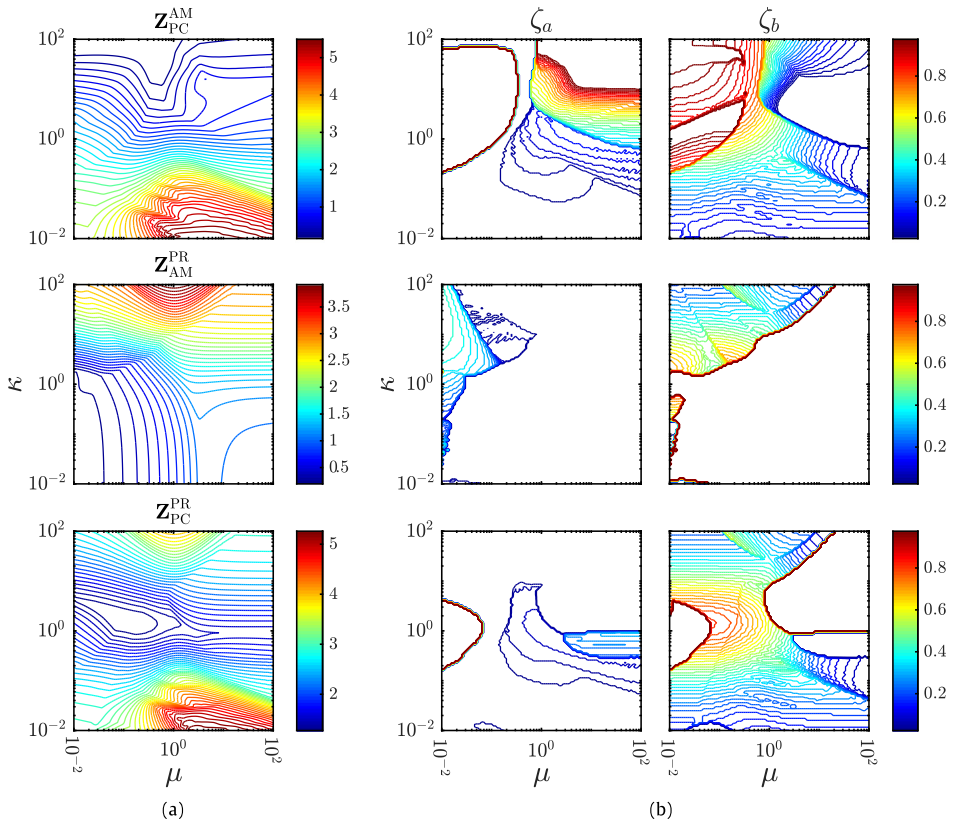

Fig. 7. (a) Optimal metadamping emergence in the metrics: $\mathbf{Z}_{\mathrm{PC}}^{\mathrm{AM}}$, $\mathbf{Z}_{\mathrm{AM}}^{\mathrm{PR}}$ and $\mathbf{Z}_{\mathrm{PC}}^{\mathrm{PR}}$ as a function of the mass and stiffness ratios, μ and κ and (b) the corresponding ζ_a and ζ_b values.

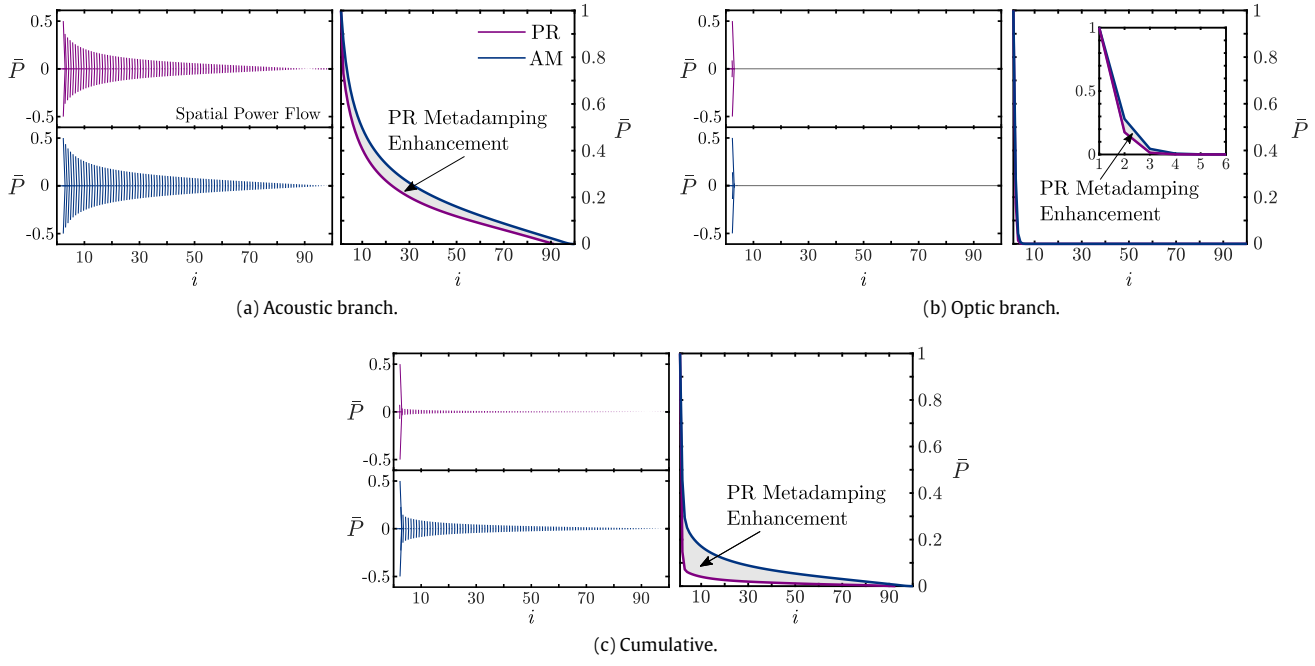

Fig. 8. Flow diagrams of the spatial power dissipation of an AM and a PR for frequencies spanning (a) the acoustic dispersion mode, (b) the optic mode, and (c) the cumulative effect.

3.2. Power flow

The previous analysis is dispersion based and thus reflects metadamping enhancements in theoretically infinite realizations of a PR compared to infinite AMs and PCs. For completion, we briefly extend the investigation to finite systems and present an evaluation of the damping performance in the context of spatial power flow dissipation. For simplicity, we exclude the PC from the comparison since it exhibits the minimal metadamping effect. We consider a PR and an AM consisting of 100 cells and adopt the

structural intensity approach (SIA) to compute the rate of energy transport along the length of both systems [36,37]. A detailed account of SIA calculations in periodic systems can be also found in [12]. At steady state, the complex frequency-dependent structural intensity of the ith mass in the PR can be obtained from

$$I_i(\omega) = -\frac{1}{2}\mathbb{i}\omega F_i^*(\omega)u_i(\omega) = P(\omega) + \mathbb{i}Q(\omega) \tag{16}$$

where $F_i^*(\omega)$ is the complex conjugate of the force in the ith spring and $u_i(\omega)$ is the displacement of the ith mass. Eq. (16) can be decomposed to its imaginary and real components to obtain the active (dissipative) $P(\omega)$ and reactive power $Q(\omega)$ components, respectively. The finite PR and AM systems are excited with a frequency-sweeping force at the first cell. Fig. 8 displays the spatial power dissipation in both the PR and the AM for the acoustic and optic bands as well as the cumulative effect on both modes. $\bar{P}$ is the active power component normalized to the maximum value for each case. Matching the expectations of Fig. 4b, the flow diagrams show faster power dissipation in the PR across both dispersion modes. The optic mode understandably shows a faster decay envelope given the higher excitation frequencies. The shaded area quantitatively reflects the metadamping enhancement in the PR system for appropriately chosen parameters.

4. Conclusion

This letter reports the dispersion characteristics of the phononic resonator (PR); a hybrid metamaterial configuration that consists of base substructures that are simultaneously connected via (1) direct elastic components and (2) local mechanical resonators. The PR design possesses qualitative properties in its band structure that can resemble phononic crystals (PCs), acoustic metamaterials (AMs), homogeneous systems, as well as its unique dispersive attributes. Upon comparing the damping performance of the PR to that of statically equivalent PC and AM configurations with identical damping amounts, it was demonstrated that the newly emergent damping capacity of the system, or the metadamping effect, of the PR can be larger than its counterparts for certain mass and stiffness ratios. Following a brief optimization analysis, the theoretically predicted metadamping enhancement is validated in finite phononic resonators via a power flow approach which illustrates the faster spatial energy attenuation in the optimized PR across frequencies corresponding to both the acoustic and optic dispersion modes.

Acknowledgment

The authors would like to acknowledge the support of the US National Science Foundation under award CMMI-1647744.

Appendix A. Dispersion derivations

We start by deriving the equations of motion for the phononic resonator (PR)

$$m_a\ddot{u}_i + c_a(2\dot{u}_i - \dot{u}_{i+1} - \dot{u}_{i-1}) + k_a(2u_i - u_{i+1} - u_{i-1}) - c_b(\dot{v}_{i+1} + \dot{v}_i - 2\dot{u}_i) - k_b(v_{i+1} + v_i - 2u_i) = 0 \tag{A.1a}$$

$$m_b\ddot{v}_i + 2c_b\dot{v}_i + 2k_bv_i - c_b(\dot{u}_{i-1} + \dot{u}_i) - k_b(u_{i-1} + u_i) = 0 \tag{A.1b}$$

Substituting the generalized Bloch-wave solution, $u_{i+r} = \tilde{u}e^{i(\beta x + r\bar{\beta}) + \lambda t}$ and $v_{i+r} = \tilde{v}e^{i(\beta x + r\bar{\beta}) + \lambda t}$, into the previous equations and rewriting in matrix form yields

$$\begin{bmatrix} \lambda^2 m_a + 2(c_b + c_a\alpha)\lambda + 2(k_b + k_a\alpha) & -k_b(e^{i\bar{\beta}} + 1) - c_b(e^{i\bar{\beta}} + 1)\lambda \\ -k_b(e^{-i\bar{\beta}} + 1) - c_b(e^{-i\bar{\beta}} + 1)\lambda & \lambda^2 m_b + 2c_b\lambda + 2k_b \end{bmatrix} \begin{Bmatrix} \tilde{u} \\ \tilde{v} \end{Bmatrix} = \begin{Bmatrix} 0 \\ 0 \end{Bmatrix} \tag{A.2}$$

where $\alpha = (1 - \cos\bar{\beta})$. Taking the determinant of the matrix in Eq. (A.2) generates the dispersion relation

$$\lambda^4 + a\lambda^3 + b\lambda^2 + c\lambda + d = 0 \tag{A.3}$$

The expressions of a, b, c and d in Table A.2 can be then rewritten in non-dimensional form as given in the manuscript.

Appendix B. Extrema of the dispersion relations

The analysis presented here is for the undamped PR, which has the following dispersion relation

$$\Omega^4 - (2(1+\mu) + 2\gamma\alpha)\Omega^2 + (4\gamma + 2\mu)\alpha = 0 \tag{B.1}$$

Substituting $\bar{\beta} = 0$ into α the dispersion relation Eq. (B.1) produces two solutions to the acoustic and optical branches, which are given by

$$\Omega = 0 \tag{B.2a}$$

$$\Omega = \sqrt{2(1+\mu)} \tag{B.2b}$$

Similarly, two additional solutions are obtained by substituting $\bar{\beta} = \pi$, resulting in the following equation

$$\Omega^4 - (2(1+\mu) + 4\gamma)\Omega^2 + 4(2\gamma + \mu) = 0 \tag{B.3}$$

which has two roots

$$\Omega_\pm^2 = \frac{(2(1+\mu) + 4\gamma) \pm \sqrt{(2(1+\mu) + 4\gamma)^2 - 16(2\gamma + \mu)}}{2} \tag{B.4}$$

After further manipulation, the roots of the equations can be reduced to

$$\Omega_\pm^2 = ((1+\mu) + 2\gamma) \pm \sqrt{(1 + \frac{2}{\kappa})^2(\mu - \frac{1}{1 + \frac{2}{\kappa}})^2} \tag{B.5}$$

which can be reduced to

$$\Omega_+ = \sqrt{2\mu(\frac{2}{\kappa} + 1)} \tag{B.6a}$$

$$\Omega_- = \sqrt{2} \tag{B.6b}$$

Appendix C. Switching point of a PR

The solutions of the dispersion curve at $\bar{\beta} = 0$ and $\bar{\beta} = \pi$ presented earlier determine the limits of the band gap of the PR depending on whether it behaves like a PC or an AM. Here, we determine the point at which the behavior of the PR optic branch switches from that of an AM to a PC which corresponds to the optic branch being perfectly flat. The condition is obtained by equating Eq. (B.6a) to Eq. (B.2b), resulting in

$$\mu = \frac{\kappa}{2} \tag{C.1}$$

If $\mu < \frac{\kappa}{2}$, the system behaves as a PC while if $\mu > \frac{\kappa}{2}$ it resembles an AM. There are two scenarios for the order of the band gap limits in the case of PC behavior. If Ω_+ in Eq. (B.6) is part of the optic band, then $\Omega_+ > \sqrt{2}$, hence $2\mu(\frac{2}{\kappa} + 1) > 2$ has to be satisfied, resulting in the following condition

$$\mu < \frac{\kappa}{2 + \kappa} \tag{C.2}$$

The condition in Eq. (C.2) is a subset of $\mu < \frac{\kappa}{2}$ and if it is not satisfied, then $\Omega = \sqrt{2}$ becomes the upper band gap limit. Interestingly, if $\mu = \frac{\kappa}{2+\kappa}$ the band gap vanishes and the optic

Table A.2
Expressions for a, b, c, and d for all systems [6].

	PR	PC	AM
a	$\frac{2c_b(m_a+m_b)+2c_am_b\alpha}{m_am_b}$	$\frac{(m_a+m_b)(c_a+c_b)}{m_am_b}$	$\frac{c_b(m_a+m_b)+2c_am_b\alpha}{m_am_b}$
b	$\frac{2k_b(m_a+m_b)+2(k_am_b+2c_ac_b+c_b^2)\alpha}{m_am_b}$	$\frac{(k_a+k_b)(m_a+m_b)+2c_ac_b\alpha}{m_am_b}$	$\frac{k_b(m_a+m_b)+2(k_am_b+c_ac_b)\alpha}{m_am_b}$
c	$\frac{4(c_ak_b+k_ac_b+c_bk_b)\alpha}{m_am_b}$	$\frac{2(c_ak_b+k_ac_b)\alpha}{m_am_b}$	$\frac{2(c_ak_b+k_ac_b)\alpha}{m_am_b}$
d	$\frac{2k_b(2k_a+k_b)\alpha}{m_am_b}$	$\frac{2k_bk_a\alpha}{m_am_b}$	$\frac{2k_bk_a\alpha}{m_am_b}$

and acoustic bands merge at $\bar{\beta} = \pi$, which is equal to $\Omega = \sqrt{2}$. This latter scenario mimics the behavior of a uniform lattice. If the system behaves like an AM, the upper limit is always equal to Eq. (B.6a) and the lower limit is $\Omega = \sqrt{2}$. In all these cases, it can be shown that one limit of the band gap has to be located at $\Omega = \sqrt{2}$.

Appendix D. Maximum attenuation

Examining the derivative of the reverse problem gives the maxima of the dispersion relation in Eq. (B.1). Solving for $\bar{\beta}$ in Eq. (B.1), we obtain

$$\bar{\beta} = \cos^{-1}\Phi \tag{D.1}$$

where

$$\Phi = 1 - \frac{\Omega^4 - 2(1+\mu)\Omega^2}{\frac{2\mu}{\kappa}\Omega^2 - (\frac{4\mu}{\kappa} + 2\mu)} \tag{D.2}$$

The derivative of Eq. (D.2) with respect to Ω is found to be

$$\frac{d\Phi}{d\Omega} = (\frac{2\mu}{\kappa}\Omega^2 - (\frac{4\mu}{\kappa} + 2\mu))(4\Omega^3 - 4(1+\mu)\Omega) - (\Omega^4 - 2(1+\mu)\Omega^2)(\frac{4\mu}{\kappa}\Omega) \tag{D.3}$$

After further manipulation, we get

$$\frac{d\Phi}{d\Omega} = \Omega\big(\Omega^4 - 4(1+\frac{\kappa}{2})\Omega^2 + 4(1+\mu)(1+\frac{\kappa}{2})\big) \tag{D.4}$$

If the derivative is set to zero, $\Omega = 0$ is a solution, which is a minimum, and the following quadratic formula represents the remaining roots

$$\Omega^2 = \frac{4(1+\frac{\kappa}{2}) \pm \sqrt{16(1+\frac{\kappa}{2})^2 - 16(1+\mu)(1+\frac{\kappa}{2})}}{2} \tag{D.5}$$

Simplifying the roots further, we finally obtain

$$\Omega^2 = (2+\kappa) \pm \sqrt{(2+\kappa)(\kappa - 2\mu)} \tag{D.6}$$

Appendix E. Long wave speed

The undamped long wave speed, or c_{stat}, is calculated from the acoustic branch of the dispersion curve which, for PR case, is given by

$$\Omega_1 = \sqrt{1+\mu+\gamma\alpha - \sqrt{(1+\mu+\gamma\alpha)^2 - 2(2\gamma+\mu)}} \tag{E.1}$$

where $\alpha = \sin^2\frac{\bar{\beta}}{2}$. Here, two approximations for the dispersion relation are used. The first is a binomial approximation $(1+\chi)^\epsilon \simeq 1 + \epsilon\chi$, when $\chi \ll 1$ and the second is a Taylor series expansion. If the dispersion relation is written in the following form

$$\Omega = \sqrt{\big((1+\mu) + 2\gamma\sin^2\frac{\bar{\beta}}{2}\big)\big(1 - \sqrt{1+\chi}\big)} \tag{E.2}$$

where

$$\chi = -4\frac{(2\gamma+\mu)\sin^2\frac{\bar{\beta}}{2}}{\big((1+\mu) + 2\gamma\sin^2\frac{\bar{\beta}}{2}\big)^2} \tag{E.3}$$

then the value of $\epsilon = \frac{1}{2}$ and $1 - \sqrt{1+\chi}$ simplifies to:

$$1 - \sqrt{1+\chi} \simeq -\frac{1}{2}\chi = 2\frac{(2\gamma+\mu)\sin^2\frac{\bar{\beta}}{2}}{\big((1+\mu) + 2\gamma\sin^2\frac{\bar{\beta}}{2}\big)^2} \tag{E.4}$$

which yields

$$\Omega^2 \simeq 2\frac{(2\gamma+\mu)\sin^2\frac{\bar{\beta}}{2}}{(1+\mu) + 2\gamma\sin^2\frac{\bar{\beta}}{2}} \tag{E.5}$$

A second order Taylor series approximation around $\bar{\beta} = 0$ is needed to further reduce the equation. If Eq. (E.5) is written as $\frac{\alpha_1\theta^2}{\alpha_2+\alpha_3\theta^2}$, the Taylor series approximation gives

$$f(\theta) \simeq \frac{\alpha_1}{\alpha_2}\theta^2 \tag{E.6}$$

where $\alpha_1 = 4\gamma + 2\mu$, $\alpha_2 = 1+\mu$, $\alpha_3 = 2\gamma$ and $\theta = \sin\frac{\bar{\beta}}{2}$. Hence Eq.(E.5) becomes

$$\Omega^2 \simeq \frac{4\gamma+2\mu}{1+\mu}\sin^2\frac{\bar{\beta}}{2} \tag{E.7}$$

It is established that the small-angle approximation for $\sin^2\frac{\bar{\beta}}{2} = \frac{\bar{\beta}^2}{4}$. Therefore, the final approximation of the acoustic branch around $\bar{\beta} = 0$ in the dimensional form is

$$\omega \simeq \omega_0^{\mathrm{PR}}\beta\ell\sqrt{\frac{\gamma + \frac{\mu}{2}}{1+\mu}} \tag{E.8}$$

Finally, the derivative with respect to the wavenumber β can be applied to find the initial slope of the acoustic dispersion band

$$c_{stat}^{\mathrm{PR}} \simeq \frac{\partial\omega}{\partial\beta} \simeq \omega_0^{\mathrm{PR}}\ell\sqrt{\frac{\gamma+\frac{\mu}{2}}{1+\mu}} = \omega_0^{\mathrm{PR}}\ell\sqrt{\frac{\mu(\kappa+2)}{2\kappa(1+\mu)}} \tag{E.9}$$

A similar process can be followed for an undamped AM, as the AM dispersion relation has similar formulation of PR. The only difference is that the AM dispersion relation has different coefficients, which are $\alpha_1 = 4\gamma$, $\alpha_2 = 1+\mu$, and $\alpha_3 = 4\gamma$. The final form of the equation is given by

$$c_{stat}^{\mathrm{AM}} = \omega_0^{\mathrm{AM}}\ell\sqrt{\frac{\mu}{\kappa(1+\mu)}} \tag{E.10}$$

An undamped PC, however, has a different form than that of PR or AM, where the acoustic branch solution is given by

$$\Omega_1 = \sqrt{\frac{(1+\mu)(1+1/\kappa)}{2} - \sqrt{\frac{(1+\mu)^2(1+1/\kappa)^2}{4} - 2\gamma\alpha}} \tag{E.11}$$

After writing the dispersion relation in a similar form as that of Eq. (E.2), we get

$$\Omega_1 = \sqrt{\alpha_1\big(1 - \sqrt{1+\chi}\big)} \tag{E.12}$$

where $\chi = -\frac{2\gamma}{\alpha_1^2}\alpha$ and $\alpha_1 = \frac{(1+\mu)(1+1/\kappa)}{2}$. Applying the binomial approximation, while assuming small angles, results in

$$\Omega_1 \simeq \sqrt{\frac{\gamma}{(1+\mu)(1+1/\kappa)}}\bar{\beta} \tag{E.13}$$

Writing the frequency in dimensional from, and with further manipulation, simplifies the equation to

$$\omega \simeq \omega_0^{\mathrm{PC}} \beta \ell \sqrt{\frac{\mu}{(1+\mu)(1+\kappa)}} \tag{E.14}$$

Finally, the derivative with respect to β yields the initial slope of the acoustic dispersion band

$$c_{stat}^{\mathrm{PC}} \simeq \frac{\partial \omega}{\partial \beta} \simeq \omega_0^{\mathrm{PC}} \ell \sqrt{\frac{\mu}{(\kappa+1)(\mu+1)}} \tag{E.15}$$

References

[1] M.I. Hussein, M.J. Leamy, M. Ruzzene, Dynamics of phononic materials and structures: Historical origins, recent progress, and future outlook, Appl. Mech. Rev. (ISSN: 0003-6900) 66 (4) (2014) 040802. http://dx.doi.org/10.1115/1.4026911.

[2] H.H. Huang, C.T. Sun, A study of band-gap phenomena of two locally resonant acoustic metamaterials, Proc. Inst. Mech. Eng. (2011) 1740349911409981.

[3] E. Baravelli, M. Ruzzene, Internally resonating lattices for bandgap generation and low-frequency vibration control, J. Sound Vib. (ISSN: 0022460X) 332 (25) (2013) 6562–6579. http://dx.doi.org/10.1016/j.jsv.2013.08.014.

[4] M. Ruzzene, F. Scarpa, F. Soranna, Wave beaming effects in two-dimensional cellular structures, Smart Mater. Struct. (ISSN: 0964-1726) 12 (2003) 363–372. http://dx.doi.org/10.1088/0964-1726/12/3/307.

[5] P. Celli, S. Gonella, Tunable directivity in metamaterials with reconfigurable cell symmetry, Appl. Phys. Lett. (ISSN: 00036951) 106 (9) (2015). http://dx.doi.org/10.1063/1.4914011.

[6] M.I. Hussein, M.J. Frazier, Metadamping: An emergent phenomenon in dissipative metamaterials, J. Sound Vib. 332 (20) (2013) 4767–4774.

[7] M. Nouh, O. Aldraihem, A. Baz, Wave propagation in metamaterial plates with periodic local resonances, J. Sound Vib. (ISSN: 10958568) 341 (2015) 53–73. http://dx.doi.org/10.1016/j.jsv.2014.12.030.

[8] H.H. Huang, C.T. Sun, G.L. Huang, On the negative effective mass density in acoustic metamaterials, Internat. J. Engrg. Sci. 47 (4) (2009) 610–617.

[9] G.L. Huang, C.T. Sun, Band gaps in a multiresonator acoustic metamaterial, J. Vib. Acoust. (ISSN: 07393717) 132 (3) (2010) 031003. http://dx.doi.org/10.1115/1.4000784.

[10] M.G. Faulkner, D.P. Hong, Free vibrations of a mono-coupled periodic system, J. Sound Vib. (ISSN: 10958568) 99 (1) (1985) 29–42. http://dx.doi.org/10.1016/0022-460X(85)90443-2.

[11] M. Nouh, On the spatial sampling and beat effects in discrete wave profiles of lumped acoustic metamaterials, J. Acoust. Soc. Am. 141 (3) (2017) 1514–1522.

[12] H.B. Al Ba'ba'a, M. Nouh, Mechanics of longitudinal and flexural locally resonant elastic metamaterials using a structural power flow approach, Int. J. Mech. Sci. 122 (2017) 341–354.

[13] H. Al Ba'ba'a, M. Nouh, An investigation of vibrational power flow in one-dimensional dissipative phononic structures, J. Vib. Acoust. 139 (2) (2017) 021003-10.

[14] P.F. Pai, Metamaterial-based broadband elastic wave absorber, J. Intell. Mater. Syst. Struct. (ISSN: 1045-389X) 21 (5) (2010) 517–528. http://dx.doi.org/10.1177/1045389X09359436.

[15] M. Ruzzene, A. Baz, Control of wave propagation in periodic composite rods using shape memory inserts, J. Vib. Acoust. (ISSN: 07393717) 122 (2) (2000) 151. http://dx.doi.org/10.1115/1.568452.

[16] D. Mead, Wave propagation and natural modes in periodic systems: I. Mono-coupled systems, J. Sound Vib. (ISSN: 0022460X) 40 (1) (1975) 1–18. http://dx.doi.org/10.1016/S0022-460X(75)80227-6.

[17] D. Mead, Markuš, Coupled flexural-longitudinal wave motion in a periodic beam, J. Sound Vib. (ISSN: 0022460X) 90 (1) (1983) 1–24. http://dx.doi.org/10.1016/0022-460X(83)90399-1.

[18] M. Nouh, O. Aldraihem, A. Baz, Vibration characteristics of metamaterial beams with periodic local resonances, J. Vib. Acoust. (ISSN: 1048-9002) 136 (6) (2014) 61012. http://dx.doi.org/10.1115/1.4028453.

[19] D.J. Mead, Vibration response and wave propagation in periodic structures, J. Eng. Ind. (ISSN: 00220817) 93 (3) (1971) 783. http://dx.doi.org/10.1115/1.3428014.

[20] D.J. Mead, Y. Yaman, The harmonic response of rectangular sandwich plates with multiple stiffening: A flexural wave analysis, J. Sound Vib. (ISSN: 10958568) 145 (3) (1991) 409–428. http://dx.doi.org/10.1016/0022-460X(91)90111-V.

[21] G. Sen Gupta, Natural flexural waves and the normal modes of periodically-supported beams and plates, J. Sound Vib. (ISSN: 0022460X) 13 (1) (1970) 89–101. http://dx.doi.org/10.1016/S0022-460X(70)80082-7.

[22] M. Nouh, O. Aldraihem, A. Baz, Periodic metamaterial plates with smart tunable local resonators, J. Intell. Mater. Syst. Struct. 27 (13) (2016) 1829–1845.

[23] M.I. Hussein, M.J. Frazier, Band structure of phononic crystals with general damping, J. Appl. Phys. 108 (9) (2010) 093506.

[24] M.J. Frazier, M.I. Hussein, Viscous-to-viscoelastic transition in phononic crystal and metamaterial band structures, J. Acoust. Soc. Am. 138 (5) (2015) 3169–3180.

[25] M.J. Frazier, M.I. Hussein, Generalized Bloch's theorem for viscous metamaterials: Dispersion and effective properties based on frequencies and wavenumbers that are simultaneously complex, C. R. Phys. 17 (5) (2016) 565–577.

[26] Y. Chen, M. Barnhart, J. Chen, G. Hu, C. Sun, G. Huang, Dissipative elastic metamaterials for broadband wave mitigation at subwavelength scale, Compos. Struct. 136 (2016) 358–371.

[27] A. Krushynska, V. Kouznetsova, M. Geers, Visco-elastic effects on wave dispersion in three-phase acoustic metamaterials, J. Mech. Phys. Solids 96 (2016) 29–47.

[28] D. Krattiger, R. Khajehtourian, C.L. Bacquet, M.I. Hussein, Anisotropic dissipation in lattice metamaterials, AIP Adv. 6 (12) (2016) 121802.

[29] F. Bloch, Über die Quantenmechanik der Elektronen in Kristallgittern, Z. Phys. (ISSN: 0044-3328) 52 (7) (1929) 555–600. http://dx.doi.org/10.1007/BF01339455.

[30] M.I. Hussein, Reduced Bloch Mode Expansion for Periodic Media Band Structure Calculations, in: Proceedings of the Royal Society of London A: Mathematical, Physical and Engineering Sciences, vol. 465, The Royal Society, 2009, pp. 2825–2848.

[31] M.J. Frazier, Dissipative Wave Propagation in Phononic Crystals and Metamaterials: Models and Analysis (Ph.D. thesis), University of Colorado at Boulder, 2015.

[32] R. Zhu, X. Liu, G. Hu, C. Sun, G. Huang, A chiral elastic metamaterial beam for broadband vibration suppression, J. Sound Vib. (ISSN: 0022460X) 333 (10) (2014) 2759–2773. http://dx.doi.org/10.1016/j.jsv.2014.01.009.

[33] Z. Liu, C.T. Chan, P. Sheng, Analytic model of phononic crystals with local resonances, Phys. Rev. B 71 (1) (2005) 014103.

[34] G. Hu, L. Tang, R. Das, S. Gao, H. Liu, Acoustic metamaterials with coupled local resonators for broadband vibration suppression, AIP Adv. 7 (2) (2017) 025211.

[35] Y. Chen, G. Hu, G. Huang, A hybrid elastic metamaterial with negative mass density and tunable bending stiffness, J. Mech. Phys. Solids 105 (2017) 179–198.

[36] L. Gavrić, G. Pavić, A finite element method for computation of structural intensity by the normal mode approach, J. Sound Vib. 164 (1) (1993) 29–43.

[37] D.-S. Cho, T.-M. Choi, J.-H. Kim, N. Vladimir, Structural intensity analysis of stepped thickness rectangular plates utilizing the finite element method, Thin-Walled Struct. 109 (2016) 1–12.